Electronic Supplementary Information

Flexible strontium-based metal-organic framework scintillation screen for high-resolution X-ray imaging

Peng-Kun Wang,[a,b,c] Wen-Fei Wang,[a,b,c] Bao-Yi Li,[a,b,c] Mei-Juan Xie,[a,b] Hong-Yi Bian,[a,b] Shuai-Hua Wang,[a,b] Fa-Kun Zheng,*[a,b] and Guo-Cong Guo*[a,b]

[a] State Key Laboratory of Structural Chemistry, Fujian Institute of Research on the Structure of Matter, Chinese Academy of Sciences, Fuzhou 350002, P. R. China

[b] Fujian Science & Technology Innovation Laboratory for Optoelectronic Information of China, Fuzhou, Fujian 350108, P. R. China

[c] University of Chinese Academy of Sciences, Beijing 100039, P. R. China

* Corresponding author to E-mail: zfk@fjirsm.ac.cn

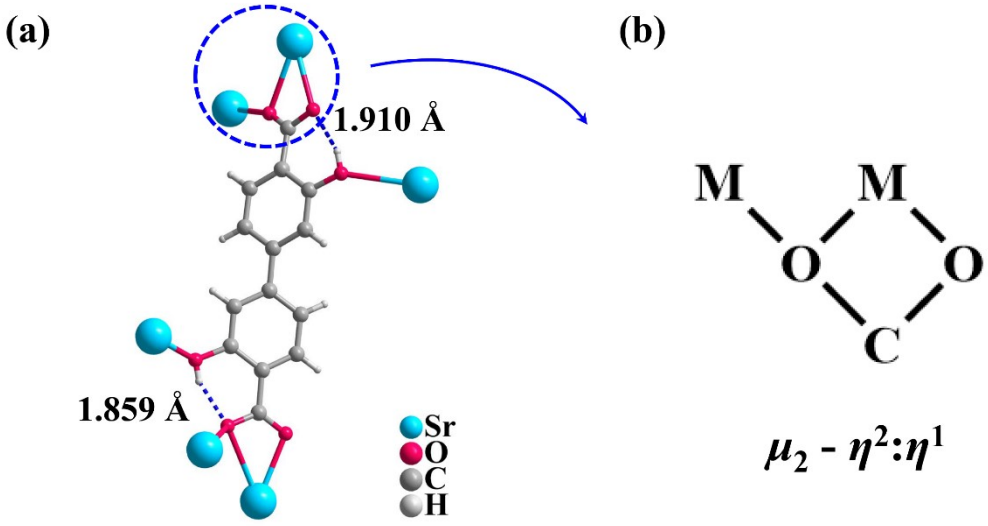

Fig. S1 (a) The coordination environment and the intramolecular hydrogen bonds of $DOBPDC^{2-}$. (b) The coordination mode of carboxylate in $DOBPDC^{2-}$.

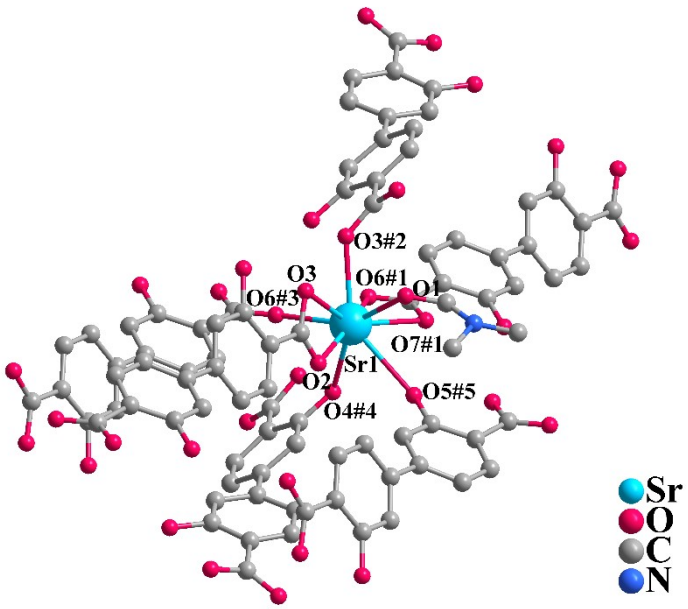

Fig. S2 The coordination environment of Sr^{2+}. For clarity, all hydrogen atoms are omitted.

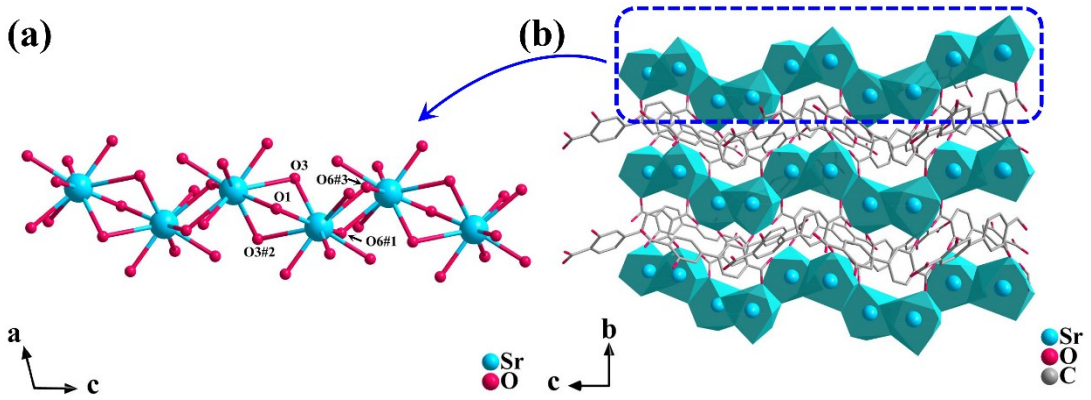

Fig. S3 (a) The 1D chain structure of **1** along the *c*-axis. (b) The 2D layer of **1** parallel to the *bc* plane. All hydrogen atoms and DMF molecules are omitted for clarity.

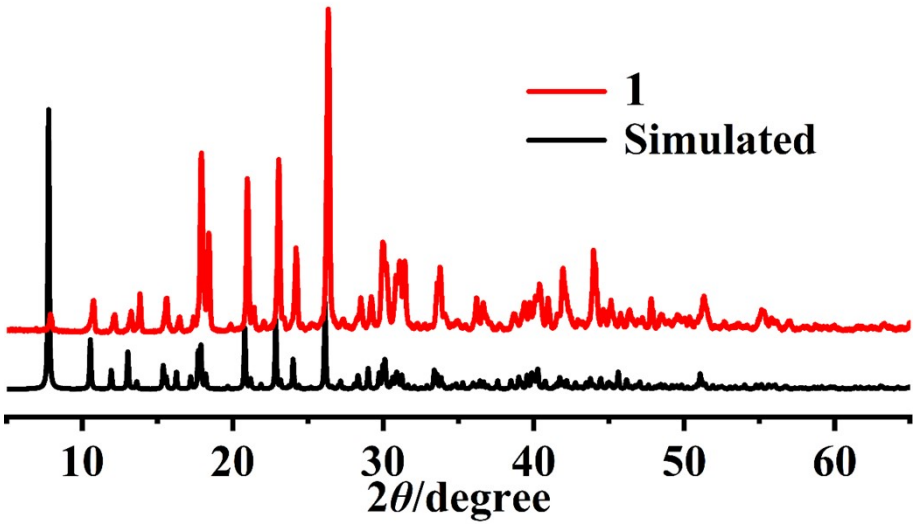

Fig. S4 The powdered X-ray diffraction (PXRD) patterns of **1**.

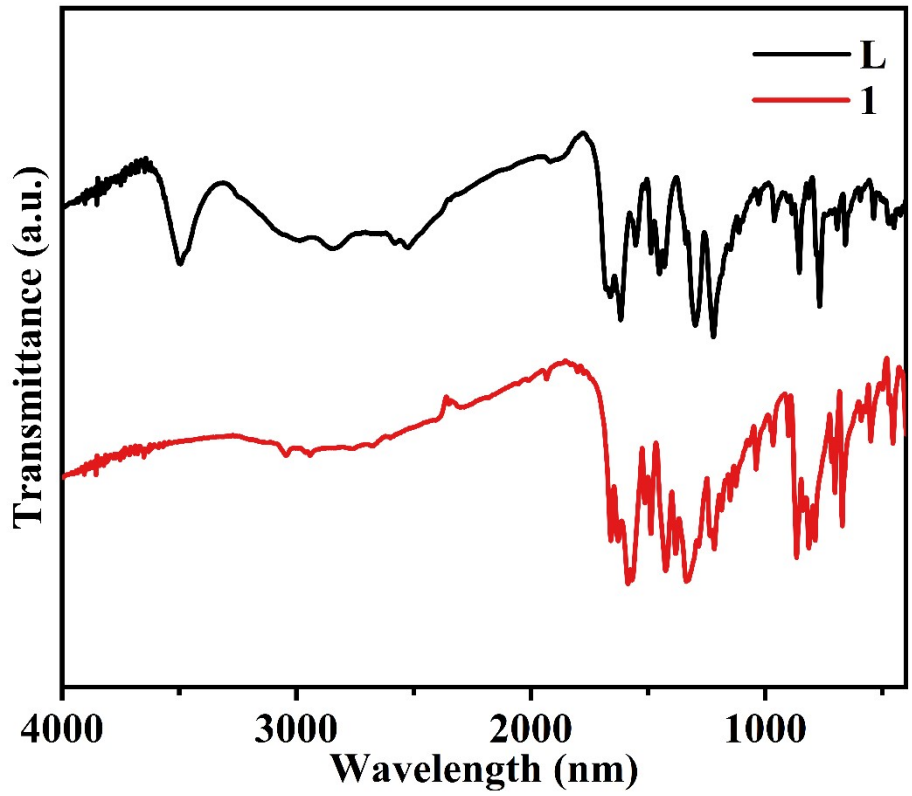

Fig. S5 The FT-IR spectra of H_2DOBPDC and **1**.

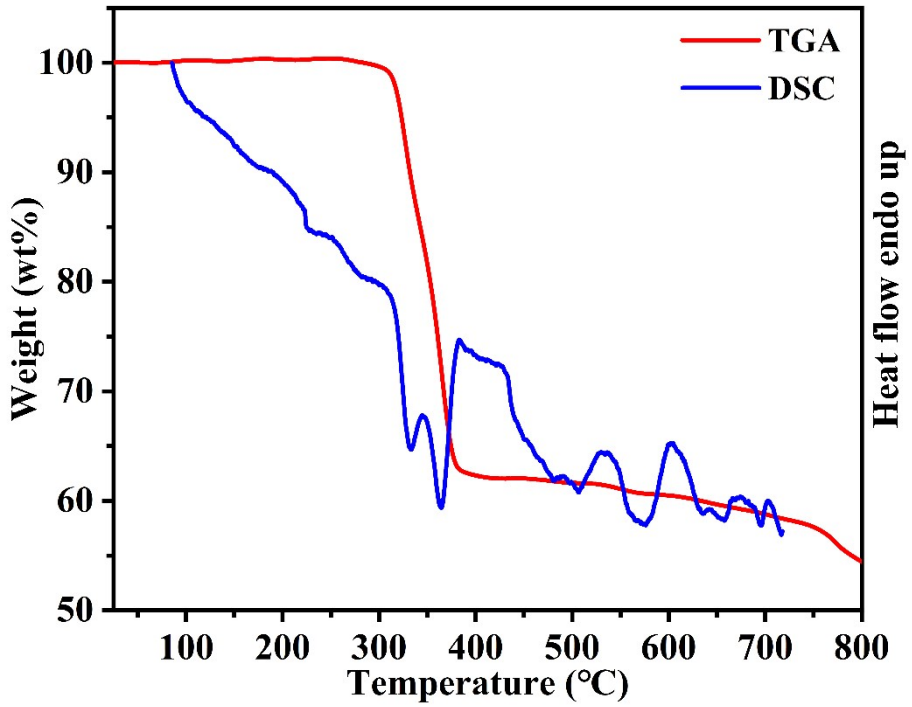

Fig. S6 The TG&DSC curves of **1**.

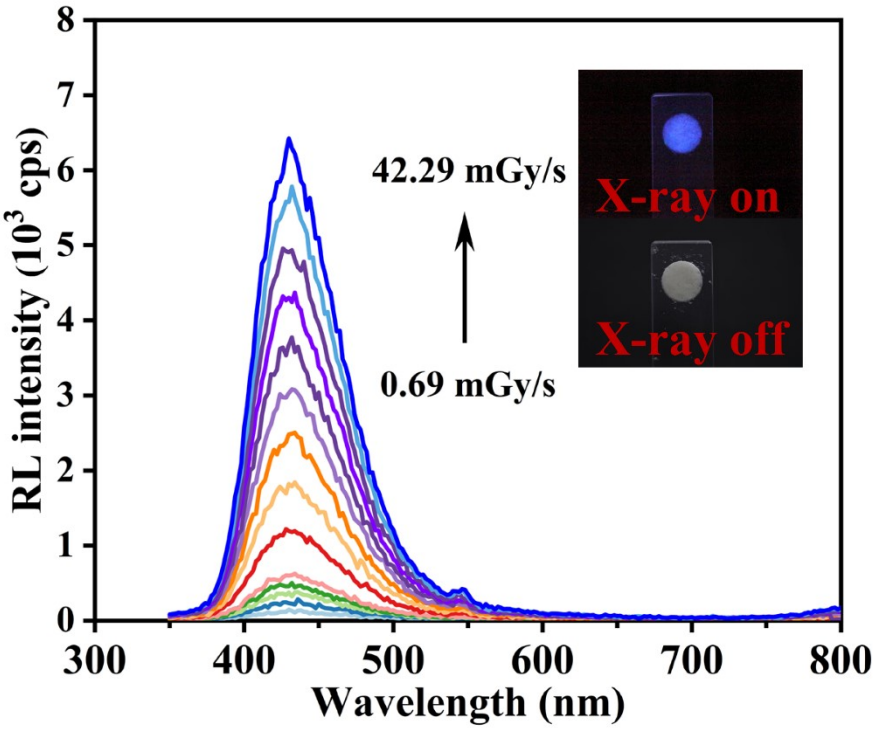

Fig. S7 X-ray dose rate dependent RL of **1** in the range of 0.69–42.29 mGy/s. The inset is the photos of **1** with X-ray on/off.

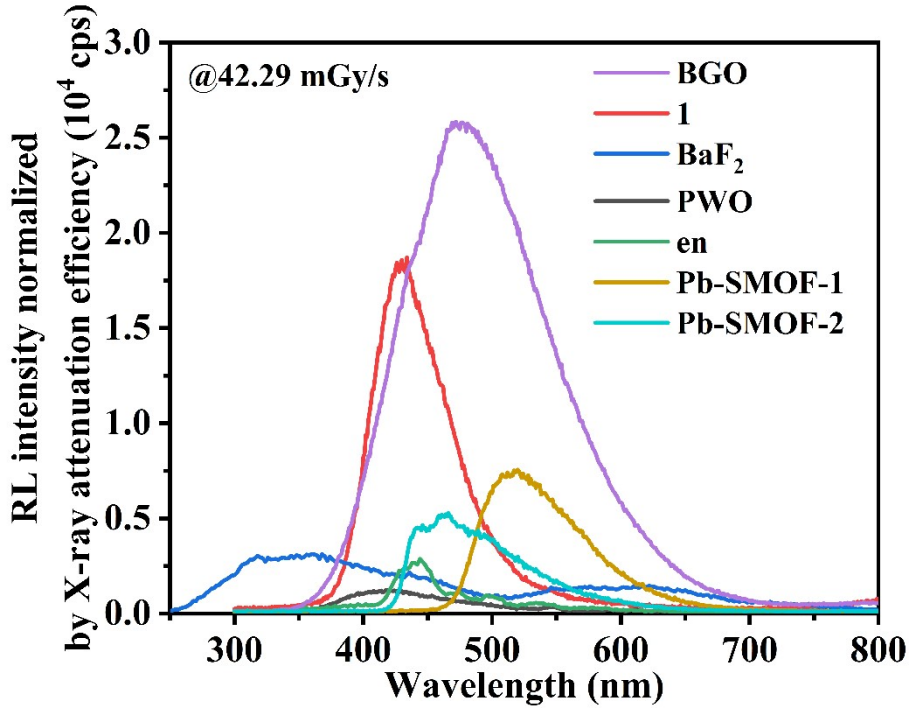

Fig. S8 The RL intensity normalized by X-ray attenuation efficiency of the samples with 2 mm of **1**, the conventional scintillators (BGO, BaF_2, PWO and organic crystal anthracene) and reported Pb-based SMOFs (Pb-SMOF-1, Pb-SMOF-2) tested at the same dose rate of 42.29 mGy/s.

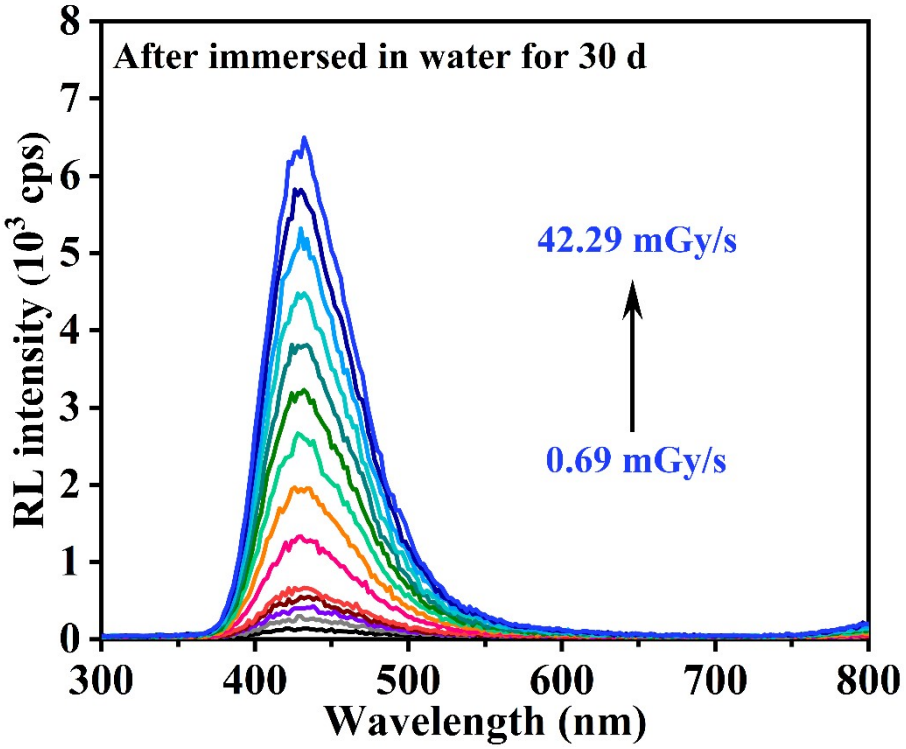

Fig. S9 The X-ray dose rate dependent RL of **1** after being immersed in water for 30 d in the range of 0.69–42.29 mGy/s.

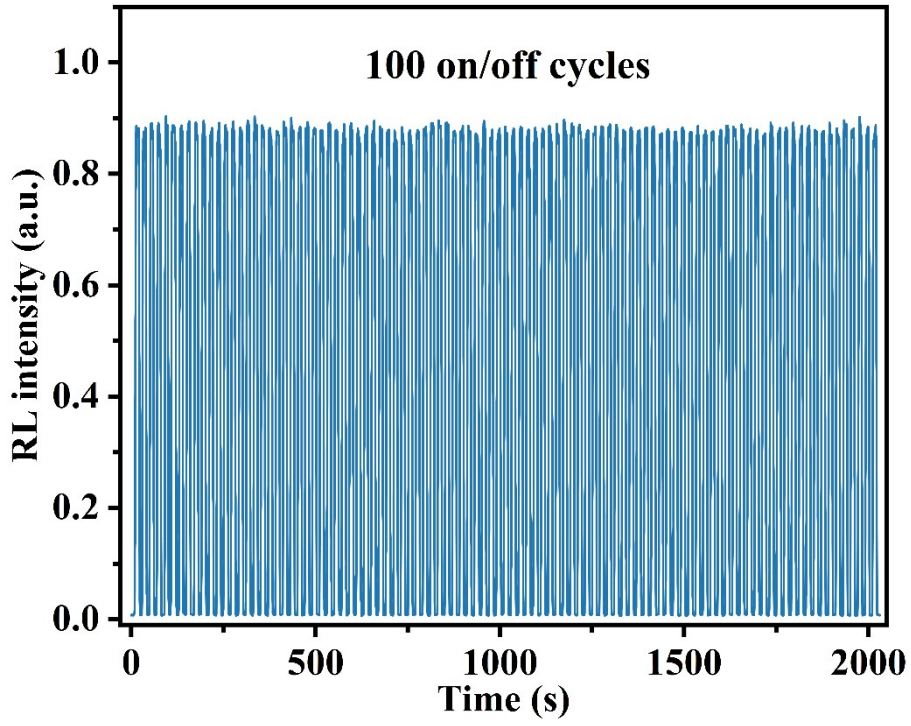

Fig. S10 RL intensities recorded for **1** over continuous 100 on/off cycles (dose rate:

42.29 mGy/s).

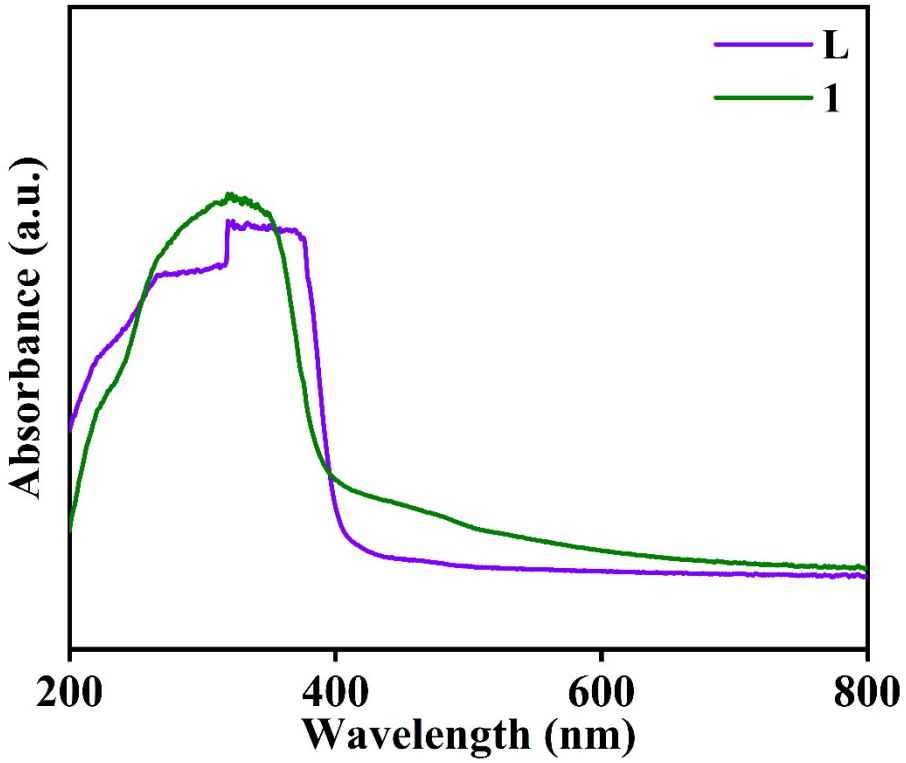

Fig. S11 The solid-state UV-Vis absorption spectra of **1** and H_2DOBPDC.

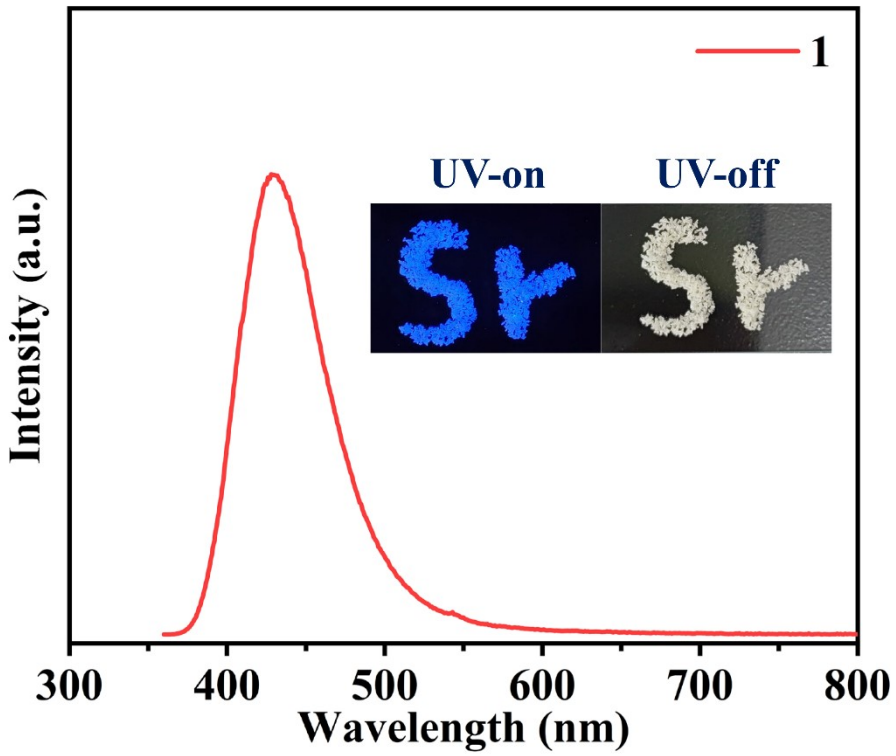

Fig. S12 The PL spectra of **1**. The inset is the photos of crystals **1** under UV light (365

nm) and in natural light, respectively.

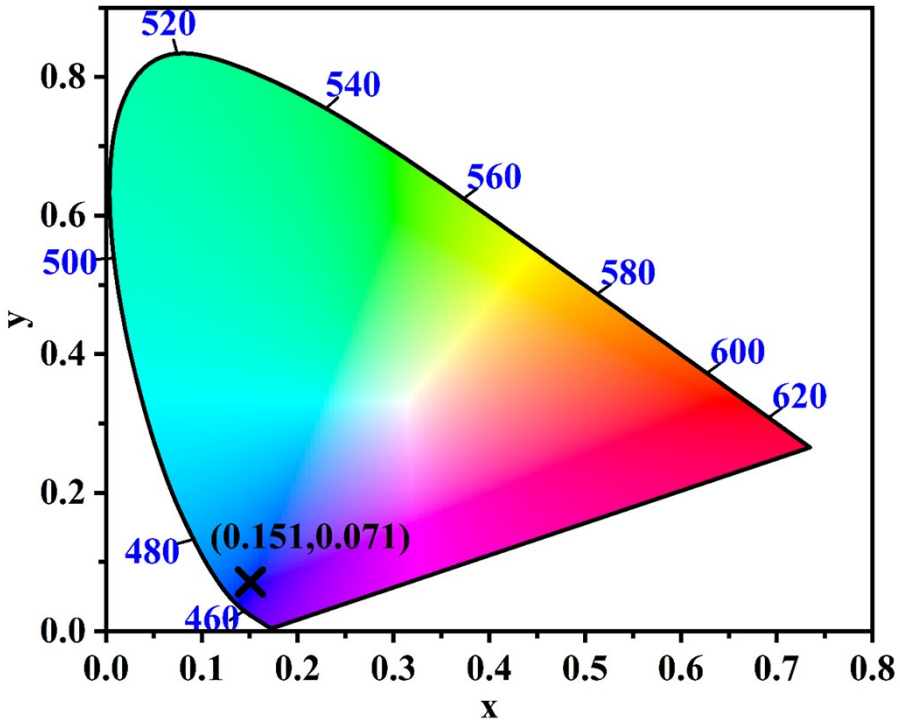

Fig. S13 Photoluminescent CIE profile of **1**

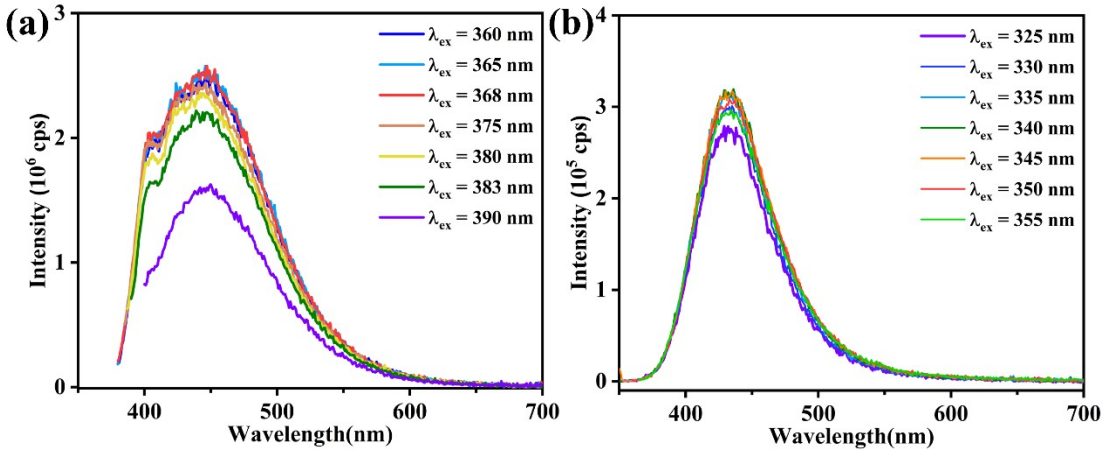

Fig. S14 (a) The solid-state PL emission spectra of H_2DOBPDC under different excitation wavelengths. (b) The solid-state PL emission spectra of **1** under different excitation wavelengths.

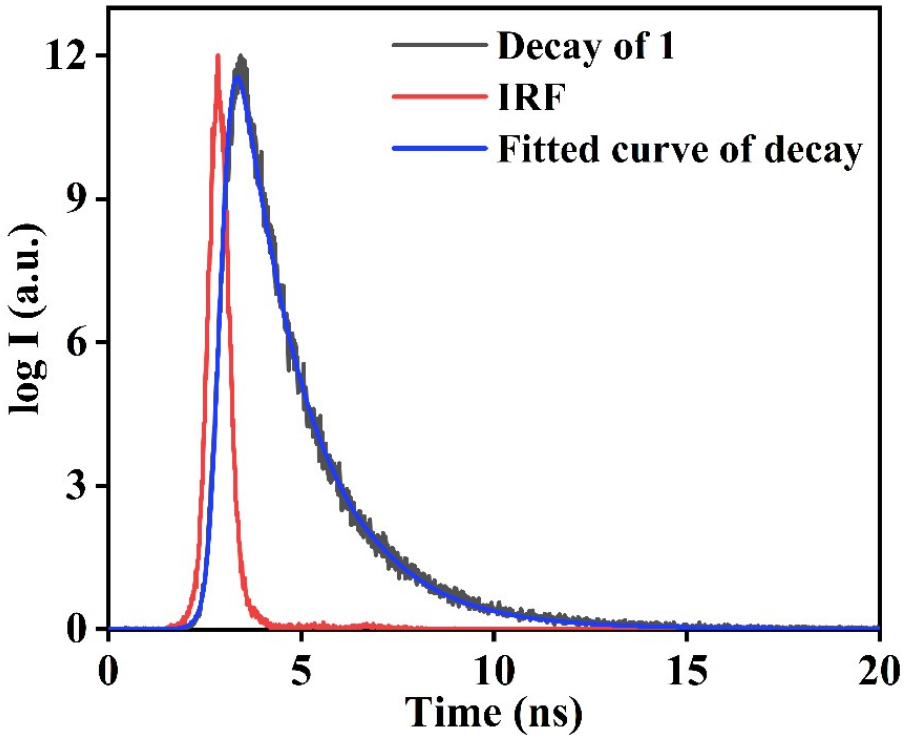

Fig. S15 PL decay time graph of solid-state **1** tested at 298 K.

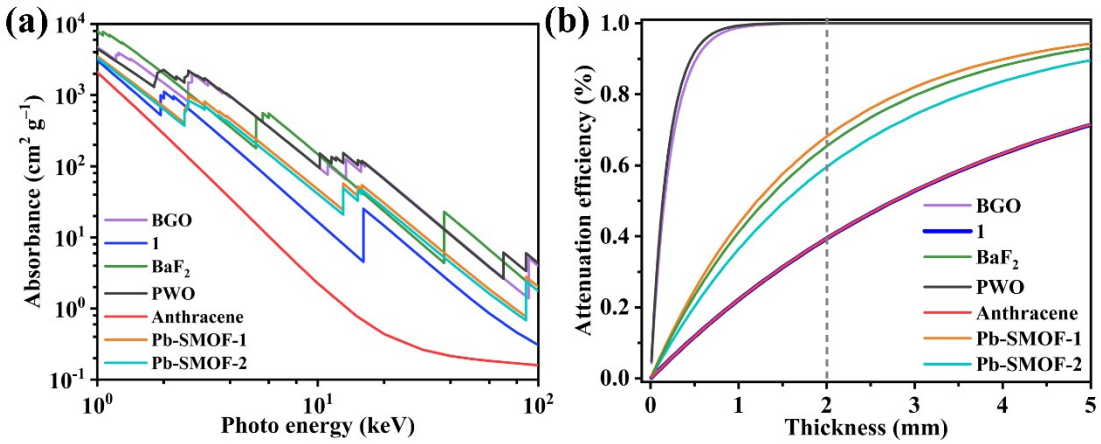

Fig. S16 (a) The simulated mass attenuation coefficient of **1** and other references as a function of the X-ray energy range from 0 to 100 keV. (b) The X-ray attenuation efficiencies as a function of the material thickness of **1** and other references toward 50 keV X-ray photons.

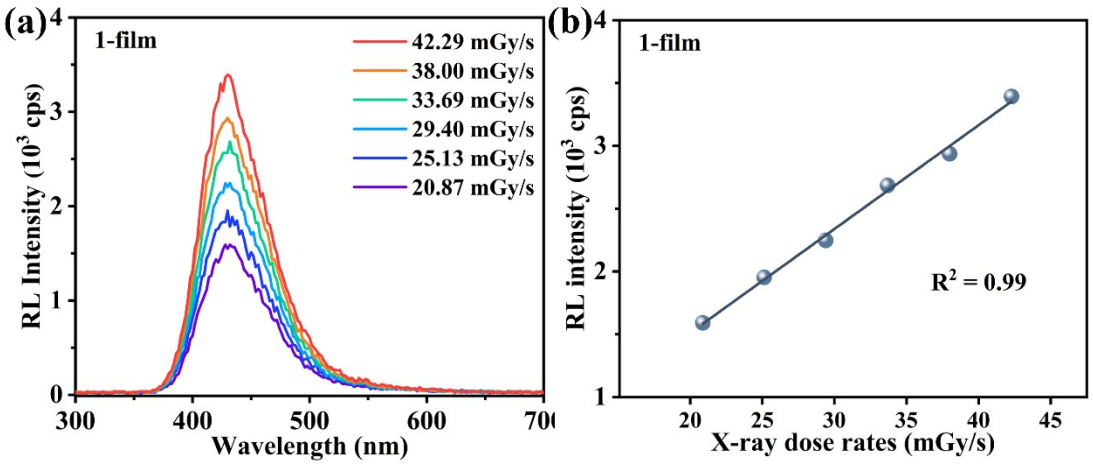

Fig. S17 (a) The X-ray dose rate dependent RL spectra of the **1-film**. (b) The RL intensity of the **1-film** *versus* the X-ray dose rate.

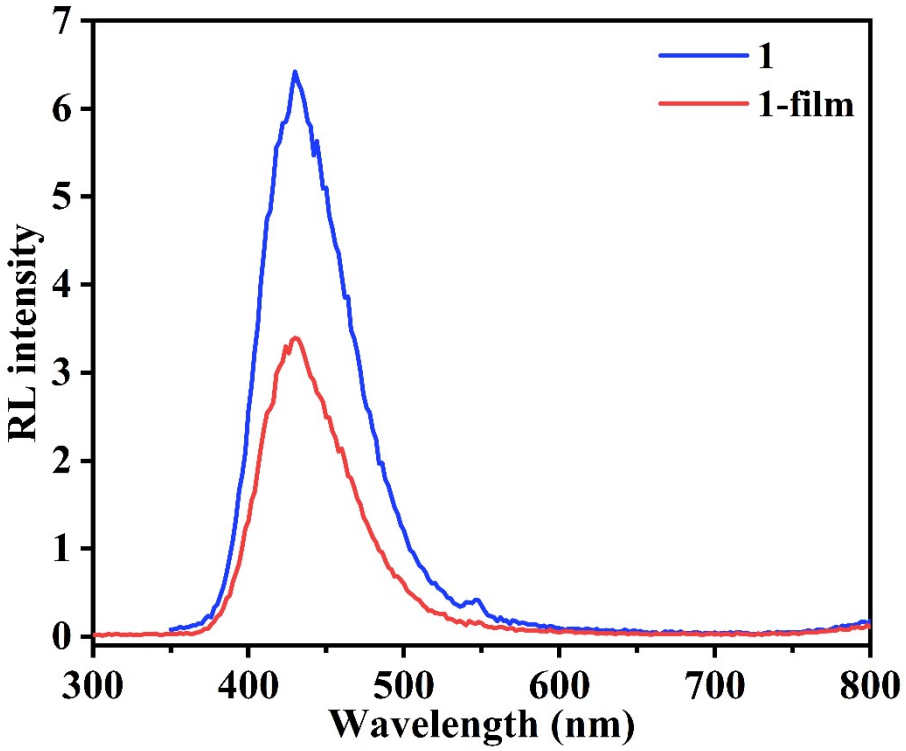

Fig. S18 The RL spectra of **1** and **1-film** at the same dose rate of 42.29 mGy/s.

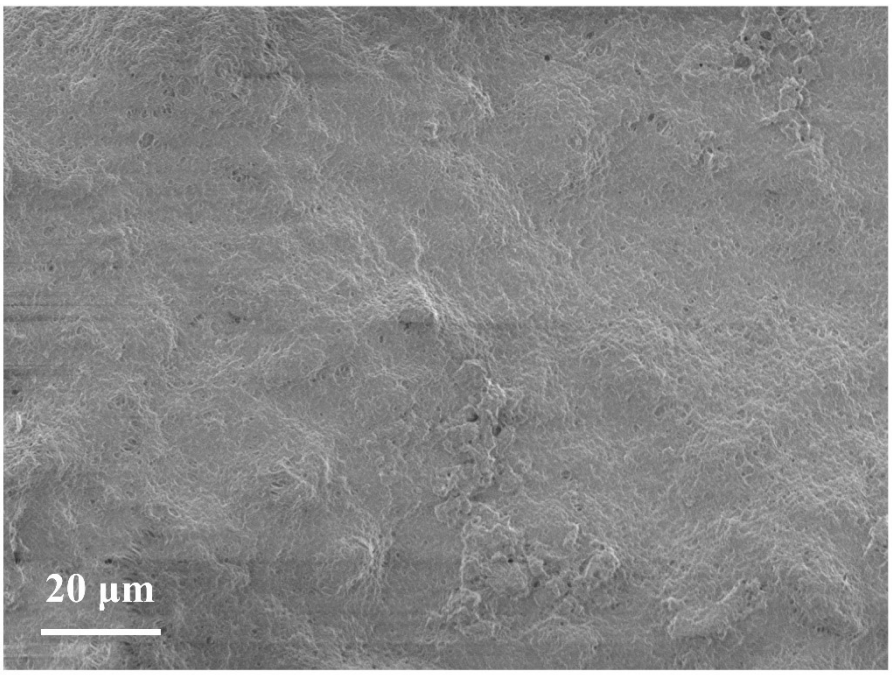

Fig. S19 The SEM photo of the **1-film**.

Fig. S20 The X-ray radiograph of curved wires under the flat **1-film**.

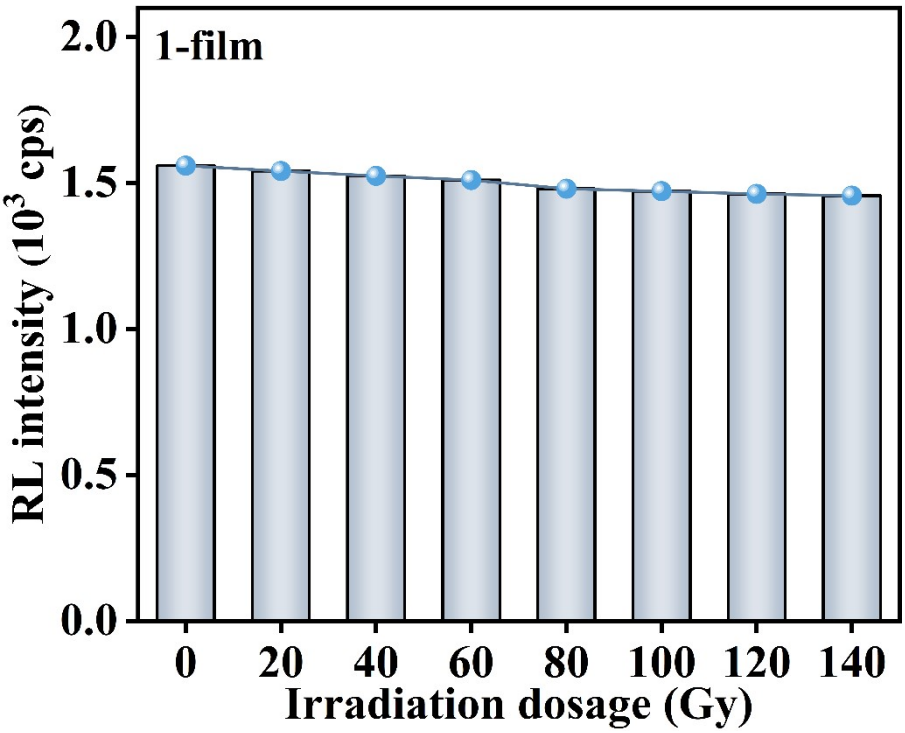

Fig. S21 The RL intensities of the **1-film** under continuous X-ray irradiation with the dose rate of 20.87 mGy/s.

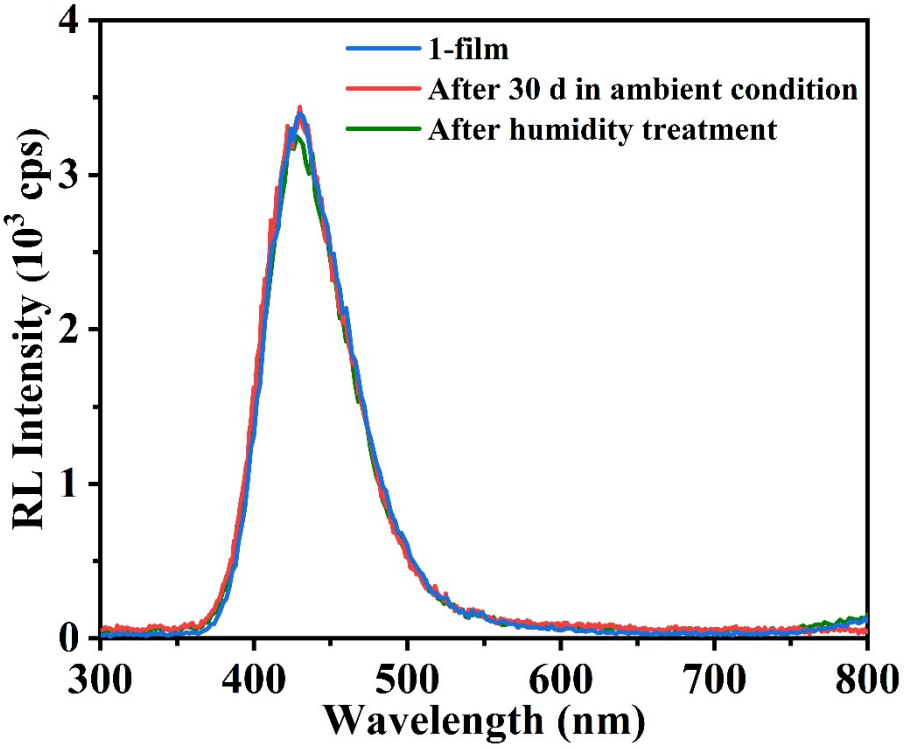

Fig. S22 The RL intensities of the **1-film**, after 30 d in ambient condition and after humidity treatment at the dose rate of 42.29 mGy/s.

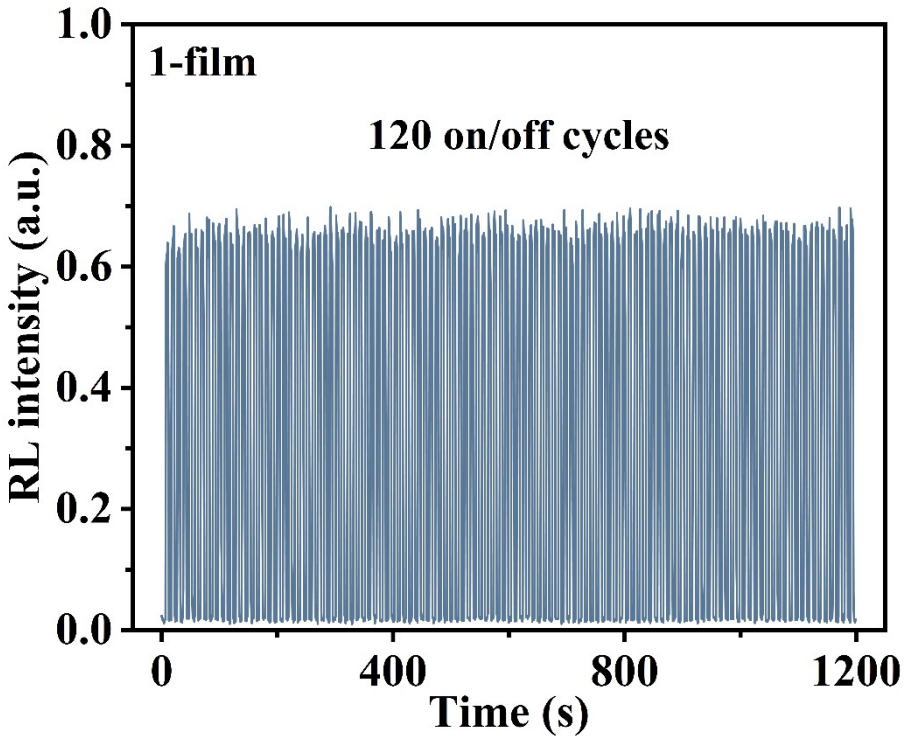

Fig. S23 The RL intensities recorded for the **1-film** over continuous 120 on/off cycles with the dose rate of 20.87 mGy/s.

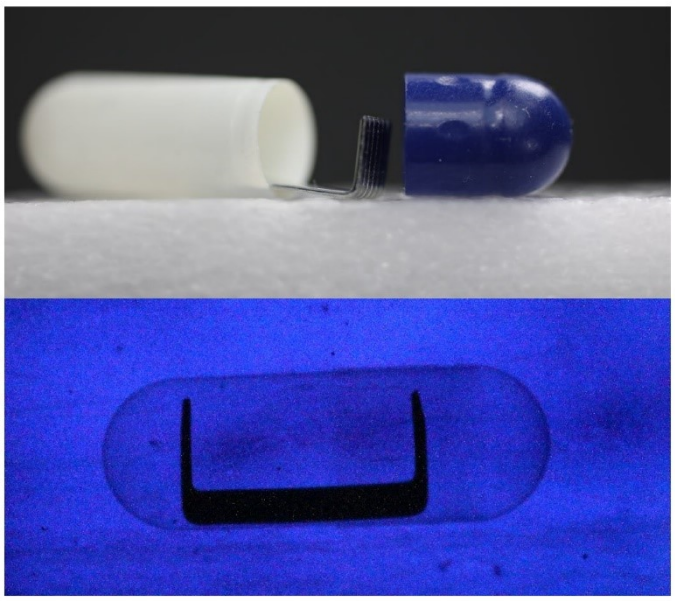

Fig. S24 The physical photo and X-ray radiograph of the **1-film** after 30 d in ambient conditions (20−35 °C, 40−65% humidity).

Table S1 Crystal data and structure refinement for **1**.

	$[Sr_2(DOBPDC)_2(DMF)]_n$
CCDC	2261586
Formula	$C_{31}H_{23}NO_{13}Sr_2$
M_r	792.74
Crystal system	monoclinic
Space group	*C2/c*
a/Å	23.5393(4)
b/Å	9.0137(2)
c/Å	13.6655(3)
α/°	90
β/°	105.235(2)
γ/°	90
V [Å^3]	2797.59(10)
Z	4
Calcd. density (g cm^{-3})	1.882
μ/mm^{-1}	5.709
F(000)	1584
2θ/°	7.786 to 153.224
Reflections collected	9232
Goodness-of-fit on F^2	1.061
Final *R* indices [$I > 2\sigma(I)$]	$R_1 = 0.0291$
	$wR_2 = 0.0756$

[a] $R_1 = \sum(F_o - F_c)/\sum F_o$. [b] $wR_2 = [\sum w(F_o^2 - F_c^2)^2/\sum w(F_o^2)^2]^{1/2}$.

Table S2 Selected bond lengths (Å) and bond angles (°) in **1**

Selected bond lengths (Å)			
Sr1–O1	2.5697(15)	Sr1–O2	2.5462(18)
Sr1–O3	2.9549(17)	Sr1–O3#1	2.6224(18)
Sr1–O4	2.660(2)	Sr1–O5#5	2.8885(18)
Sr1–O6#2	2.6037(18)	Sr1–O6#3	2.7538(17)
Sr1–O7#3	2.6171(18)		
Selected bond angles (°)			
Sr1#2–O1–Sr1	105.62(9)	O6#3–Sr1–O4#4	60.34(6)
O6#3–Sr1–O6#1	70.55(6)	O6#3–Sr1–O3	89.13(5)
O6#1–Sr1–O3	139.74(5)	O6#3–Sr1–O3#2	81.88(6)
O6#3–Sr1–O5#5	136.27(6)	O6#1–Sr1–O5#5	104.35(5)
O6#3–Sr1–O7#1	118.06(6)	O4#4–Sr1–O6#1	71.84(6)
O4#4–Sr1–O3	131.85(5)	O4#4–Sr1–O5#5	70.84(6)
O3#2–Sr1–O6#1	74.83(5)	O3#2–Sr1–O4#4	139.81(5)
O3#2–Sr1–O3	67.97(6)	O3#2–Sr1–O5#5	140.33(6)
O2–Sr1–O6#1	163.66(6)	O2–Sr1–O6#3	97.04(6)
O2–Sr1–O4#4	93.69(6)	O2–Sr1–O3#2	114.87(6)
O2–Sr1–O3	46.92(5)	O2–Sr1–O5#5	76.94(5)
O2–Sr1–O1	80.33(5)	O2–Sr1–O7#1	139.47(6)
O5#5–Sr1–O3	113.92(5)	O1–Sr1–O6#3	149.71(6)
O1–Sr1–O6#1	115.80(4)	O1–Sr1–O4#4	143.68(6)
O1–Sr1–O3	66.91(5)	O1–Sr1–O3#2	72.28(5)
O1–Sr1–O5#5	72.92(6)	O1–Sr1–O7#1	78.69(6)
O7#1–Sr1–O6#1	48.50(5)	O7#1–Sr1–O4#4	83.48(7)
O7#1–Sr1–O3	143.57(6)	O7#1–Sr1–O3#2	90.99(6)
Sr1#3–O6–Sr1#6	109.46(6)	O7#1–Sr1–O5#5	63.90(6)
Sr1#2–O3–Sr1	94.27(5)		

Symmetry codes: #1 $-1/2 + x$, $1/2 + y$, $-1 + z$; #2 $1 - x$, y, $1/2 - z$; #3 $3/2 - x$, $1/2 - y$, 1

$-z$; #4 x, $1-y$, $-1/2+z$; #5 $3/2-x$, $3/2-y$, $1-z$; #6 $1/2+x$, $-1/2+y$, $1+z$.